Charles University in Prague
Faculty of Mathematics and Physics

Summary of doctoral thesis

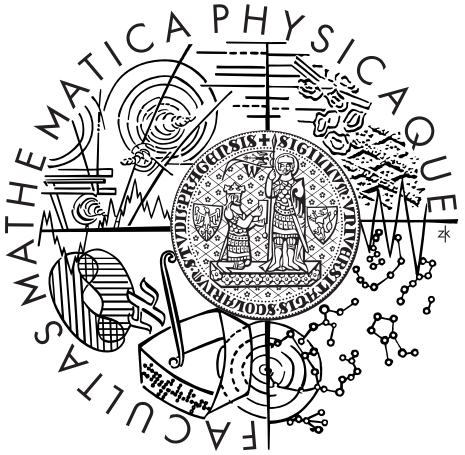

Klára Kalousová

Dynamics of icy satellites with a liquid phase

Department of Geophysics

Supervisors of the doctoral thesis:	Doc. RNDr. Ondřej Čadek, CSc. Dr. Gaël Choblet
Study programme:	Physics
Specialization:	Geophysics

Prague 2014

Univerzita Karlova v Praze
Matematicko-fyzikální fakulta

Autoreferát dizertační práce

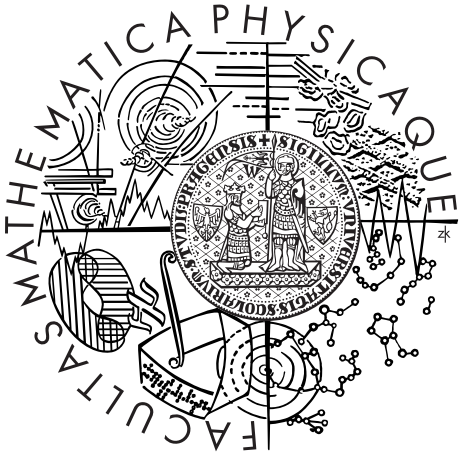

Klára Kalousová

Modelování dynamiky ledových měsíců s kapalnou fází

Katedra geofyziky

Vedoucí dizertační práce:	Doc. RNDr. Ondřej Čadek, CSc. Dr. Gaël Choblet
Studijní program:	Fyzika
Studijní obor:	Geofyzika

Praha 2014

Dizertace byla vypracována na základě výsledků získaných v letech 2010-2014 během doktorandského studia na Katedře geofyziky MFF UK a v Laboratoire de Planétologie et Géodynamique de Nantes.

Dizertant:
Mgr. Klára Kalousová
Katedra geofyziky MFF UK
V Holešovičkách 2, 180 00, Praha 8

Školitelé:
Doc. RNDr. Ondřej Čadek, CSc.
Katedra geofyziky MFF UK
V Holešovičkách 2, 180 00, Praha 8

Dr. Gaël Choblet
Laboratoire de Planétologie et Géodynamique de Nantes
2 rue de la Houssinière, F-44322, Nantes, France

Oponenti:
Dr. Hauke Hussmann
German Aerospace Center (DLR), Institute of Planetary Research
Rutherfordstrasse 2, 12489 Berlin, Germany

Dr. Yanick Ricard
Laboratoire de Géologie de Lyon
2 rue Raphael Dubois, 69622, Villeurbanne, France

Předseda oborové rady:
Doc. RNDr. Hana Čížková, Ph.D.
Katedra geofyziky MFF UK
V Holešovičkách 2, 180 00, Praha 8

Autoreferát byl rozeslán dne

Obhajoba dizertace se koná dne 26.1.2015 v 10:00 hodin před komisí pro obhajoby dizertačních prací v oboru Geofyzika v budově MFF UK, Ke Karlovu 3, Praha 2, v místnosti č. 105.

S dizertací je možno se seznámit v PGS MFF UK, Ke Karlovu 3, Praha 2.

Contents

Introduction

With its dearth of large impact craters that indicates a young surface (<100 Myr), and the abundance of various tectonic and cryovolcanic features that points to a relatively recent endogenic activity, Europa is one of the most exciting planetary bodies within our Solar System. Magnetic induction signals (*Khurana et al.*, 1998) and detection of salts on Europa's icy surface (*McCord et al.*, 1998) indicate that the moon probably possesses a salty ocean a few tens of kilometers below its surface. Morphological studies (*Schmidt et al.*, 2011; *Dombard et al.*, 2013) moreover suggest the presence of shallow water reservoirs, perched only a few kilometers below Europa's cold brittle surface, and recent detection of water vapor over Europa's south pole (*Roth et al.*, 2014) suggests the existence of an ongoing plume activity similar to that observed at Enceladus (e.g. *Hansen et al.*, 2006). Powered by tides, this endogenic activity in a chemically rich environment together with an expected ocean-mantle contact may provide the key ingredients for life (cf. *Hand et al.*, 2009), which makes Europa one of the best candidates for habitability and places it atop the interest of astrobiologists. The material exchange between the surface and the ocean, critical for potential habitability, is thus of primary interest.

In this context it is crucial to understand (i) How can meltwater be generated at shallow depth and what is its lifetime? and (ii) What processes control the water and chemical transport between the surface and the ocean? In order to address these major questions, we numerically model the mechanisms of water transport through the ice shell using two-phase flow formalism. The goal of this thesis is to investigate whether melting can initiate at shallow depths as a result of enhanced tidal heating in different geodynamical contexts, and to address the gravitational stability of these potential meltwater reservoirs with the consequences for recent morphological models.

1 Liquid water in Europa's ice shell: Observations and models

In 1610, Galileo Galilei discovered four major satellites of Jupiter (Io, Europa, Ganymede, and Callisto), which were afterwards refered to as Galilean satellites. Among them, Europa is the smallest and second in distance from Jupiter. The first three satellites are locked together in the Laplace resonance with a mean motion ratio of 4:2:1. This resonance prevents circularization of the satellites' orbits and maintains their eccentricity non-zero which leads to significant tidal deformations. The associated tidal heating is mostly located within the ice shell and may be several times larger than radiogenic heating in the rocky core (*Sotin et al.*, 2009).

With a radius of 1562 km, Europa is slightly smaller than the Moon. Gravitational data collected by the Galileo spacecraft indicate that its interior is fully differentiated into a metallic core, a silicate mantle and an outer water ice/liquid shell approximately 80–170 km thick (*Anderson et al.*, 1998). Moreover, the detection of an induced magnetic field by the Galileo magnetometer provides a very compelling evidence for the existence of an internal ocean within 200 km from the surface (*Khurana et al.*, 1998) covered by a relatively thin outer ice shell (with thickness estimates varying from a few kilometers to more than 40 km, cf. *Billings & Kattenhorn*, 2005). The state of the ice shell (convective or conductive) depends mostly on its thickness and viscosity (e.g. *Barr & Pappalardo*, 2005), however, no observations that would allow a robust assessment of the viscosity structure are available. At the surface and at shallow depths, the ice is expected to undergo a brittle failure along preexisting cracks (*Nimmo & Manga*, 2009), while at greater depths, the increased temperatures allow ductile deformation. Ice is known to have a highly nonlinear rheology, with at least four known deformational mechanisms (*Durham et al.*, 2001; *Goldsby & Kohlstedt*, 2001) and the viscosity of each mechanism depends in general on temperature, pressure, grain size, and stress. Moreover, the presence of meltwater significantly decreases the viscosity of ice matrix (*De La Chapelle et al.*, 1999).

When compared to the heavilly cratered terrains of her neighbors Ganymede and Callisto, Europa's surface displays a notable dearth of large impact craters - their size frequency distributions lead to surface age estimates that range between 40 and 90 Myr, indicating a strikingly young surface (w.r.t. the solar system time scales), consistent with current geological activity and presence of an interior ocean (*Bierhaus et al.*, 2009). While impact craters are scarce, there is an abundance of diverse tectonic and cryovolcanic surface features unique for Europa. The most common tectonic features are **double ridges** that consist of a central crack or trough flanked by two raised edifices and may extend from a few kilometers to more than 1000 km across the surface (*Kattenhorn & Hurford*, 2009). Approximately one quarter of Europa's surface is covered by **chaotic terrains** - this widespread type of terrain is formed by disruption of the preexisting surface into isolated plates (that range in size from 1 km to 20 km across) and formation of lumpy matrix material between these plates (*Carr et al.*, 1998). Several plates have moved from their original positions and some were found to have rotated and/or tilted (*Collins & Nimmo*, 2009).

Apart from the global subsurface ocean, the existence of which is now generally

accepted, liquid water might be present also within Europa's outer ice shell. Recent morphological analyses of chaos terrains (*Schmidt et al.*, 2011) and double ridges (*Dombard et al.*, 2013) as well as the UV spectra observations consistent with water vapor eruptions (*Roth et al.*, 2014) support the hypothesis of presence of liquid water within the ice shell in the form of lenses or sills located a few kilometers below the surface. However, the question of long-term stability of such subsurface water reservoirs is challenging and cannot be answered without considering meltwater generation and its subsequent propagation through the ice shell.

The production of meltwater within Europa's ice shell is considered to be the consequence of tidal heating expected presently in two main scenarios - either in thermal hot plumes as a result of thermally-reduced viscosity (*Sotin et al.*, 2002; *Tobie et al.*, 2003) or along the faults due to tidally-activated strike-slip motions (*Nimmo & Gaidos*, 2002). However, the presence of meltwater at shallow depth is largely complicated by the very low surface temperature of Europa ($\sim$100 K, e.g. *Ojakangas & Stevenson*, 1989).

While the melting processes responsible for water generation inside the ice shell appear to be relatively well studied, only little attention has so far been paid to meltwater propagation. Hydrofracturing, the drainage mechanism dominant on the Earth that typically allows for very rapid water drainage (e.g. *Krawczynski et al.*, 2009), seems unlikely to prevail in Europa's shell due to several important differences between the physical setting within the ice shell and that within the Earth's glaciers (such as the absence of subglacial drainage system, closure of the hydrological network from above, limited crack initiation, insufficient meltwater supply, or one order of magnitude difference in the thicknesses of ice masses).

If we neglect hydrofracturing and rule out voids (that are unlikely due to large overburden pressure), then any meltwater flow through the ice shell must be accompanied by a viscous deformation of the ice. Such mechanical coupling between the two phases (much stronger than in the terrestrial glaciers) must be taken into account and the problem of ice melting and subsequent meltwater propagation within the icy shells then requires the adoption of a two-phase formalism (developed originally for magma generation and transport). Considering the ice shell as a two-phase mixture of water ice and liquid water, then water, as the less viscous phase (melt), would be transported through the more viscous phase (ice matrix) by a system of interconnected channels (pores). The meltwater transport by this mechanism is expected to be predominant in sufficiently large regions of partially molten material, such as within the hot plumes.

In case of totally impermeable ice (with no cracks or pores), a third mechanism involves gravitational destabilization of large liquid water reservoirs by Rayleigh-Taylor (R-T) instabilities in the water-ice system. This instability develops at the interface between two viscous fluids of different densities. Gravitational destabilization of liquid water reservoir by R-T instability would probably require accumulation of substantial volume of meltwater underlain by sufficiently impermeable (cold) ice - otherwise, the liquid water would rather be drained by microscopic two-phase flow. This may be possible only in the vicinity of localized frictional heat sources at strike-slip faults, or in the zones with reduced melting temperature (e.g. due to presence of salts) heated from below by ascending plumes.

2 Theoretical model and numerical implementation

The two-phase (or generally multi-phase) flow has been intensively studied in geophysics, especially in connection with magma generation and lava flows (e.g. *McKenzie*, 1984; *Scott & Stevenson*, 1986), planetary core formation and segregation (e.g. *Ricard et al.*, 2009; *Šrámek et al.*, 2010), soil mechanics (e.g. *Birchwood & Turcotte*, 1994), or closer to our application, in glaciology (e.g. *Blatter & Hutter*, 1991; *Hutter*, 1993).

Despite the obvious multiscale (both temporal and spatial) nature of the above phenomena, we are often interested only in physical processes at macroscopic (or mesoscopic) scale. A substantial theoretical simplification can then be achieved by employing the framework of continuum mechanics and thermodynamics. Two main branches exist within these theories concerning multi-component processes and phenomena: (i) the mixture theory and (ii) the multi-phase theory. In this thesis, we choose the multi-phase theory which is connected with the work of *Drew* (1983) and *Drew & Passman* (1999). In this framework, the space-temporal distribution of the phases at a sufficiently fine mesoscale is assumed to be known and the traditional single-component continuum theory is assumed to be valid in the regions occupied by each phase. After the identification of suitable boundary conditions at the interfaces between the phases, the multi-component description is obtained by performing an averaging procedure (over a representative volume or statistical ensemble) which eliminates the microscale details.

In our particular application (i.e. production and transport of liquid water within the ice shell) we are interested in the behavior of partially molten ice without any additional impurities. Our multi-phase material is thus composed of only two phases - the matrix (ice, subscripted by 'm') and the fluid (water, subscripted by 'f'). To derive the averaged two-phase equations we closely followed the work of *Drew* (1983), *Drew & Passman* (1999), *Bercovici et al.* (2001) and *Šrámek et al.* (2007) and subsequently, we performed a scaling analysis appropriate for our planetary application in order to neglect the terms of small importance (such as inertial forces, viscous stresses in the fluid phase, the effects of surface tension, the momentum transfer due to phase change, or the viscous heating of both phases). These procedures led to (dimensional) balance equations of the form:

$$\frac{\partial \phi}{\partial t} - \nabla \cdot ((1-\phi)\boldsymbol{v}_\mathrm{m}) = \frac{r_\mathrm{f}}{\rho_\mathrm{m}} \ , \tag{1a}$$

$$\nabla \cdot \boldsymbol{v}_\mathrm{m} + \nabla \cdot (\phi \boldsymbol{v}_\mathrm{r}) = \frac{\Delta\rho}{\rho_\mathrm{f}\rho_\mathrm{m}} r_\mathrm{f} \ , \tag{1b}$$

$$c\boldsymbol{v}_\mathrm{r} = -\phi\nabla\Pi - \phi\Delta\rho\mathbf{g} \ , \tag{1c}$$

$$\begin{aligned}\nabla\Pi = &-\phi\Delta\rho\mathbf{g} - (1-\phi)\rho_\mathrm{m}\alpha_\mathrm{m}\Delta T\mathbf{g} + \nabla\left(\frac{(1-\phi)\mu_\mathrm{m}}{\phi}(\nabla\cdot\boldsymbol{v}_\mathrm{m})\right) \\ &+ \nabla\cdot\left((1-\phi)\mu_\mathrm{m}\left[\nabla\boldsymbol{v}_\mathrm{m} + (\nabla\boldsymbol{v}_\mathrm{m})^T - \frac{2}{3}(\nabla\cdot\boldsymbol{v}_\mathrm{m})\boldsymbol{I}\right]\right) \ ,\end{aligned} \tag{1d}$$

$$\phi\rho_\mathrm{f}c_\mathrm{f}\frac{\mathrm{D_f}T}{\mathrm{D}t} + (1-\phi)\rho_\mathrm{m}c_\mathrm{m}\frac{\mathrm{D_m}T}{\mathrm{D}t} + Lr_\mathrm{f} = Q + \nabla\cdot(k^\mathrm{T}(\phi)\nabla T) + c|\boldsymbol{v}_\mathrm{r}|^2 \ . \tag{1e}$$

Here ϕ is the porosity (volume fraction of fluid in the mixture), $\boldsymbol{v}_\mathrm{m}$ is the matrix

(ice) velocity, r_f is the melt production rate, ρ_m is the ice density, $\boldsymbol{v}_\mathrm{r}{=}\boldsymbol{v}_\mathrm{f}{-}\boldsymbol{v}_\mathrm{m}$ is the relative velocity between the two phases, $\Delta\rho{=}\rho_\mathrm{m}{-}\rho_\mathrm{f}$ is the density difference between the two phases, $c{=}\frac{\mu_\mathrm{f}\phi^2}{k(\phi)}$ is the drag coefficient with $k(\phi){=}k_0\phi^2$ the permeability and μ_f the fluid (water) shear viscosity, $\Pi{=}P_\mathrm{f}{-}P_\mathrm{m}^\mathrm{ref}$ is the excess water pressure w.r.t. the hydrostatic equilibrium pressure of pure ice ($P_\mathrm{m}^\mathrm{ref}$), $\mathbf{g}$ is the gravity, α_m is the ice thermal expansivity, $\Delta T{=}T{-}T_0$ is the temperature deviation from the reference state T_0, μ_m is the ice shear viscosity, c_f and c_m are the specific heats of fluid and matrix, respectively, L is the latent heat of the phase change, Q is the volumetric heating, $k^\mathrm{T}(\phi){=}k_\mathrm{m}^\mathrm{T}\left(1{-}\phi\frac{3(k_\mathrm{m}^\mathrm{T}-k_\mathrm{f}^\mathrm{T})}{2k_\mathrm{m}^\mathrm{T}+k_\mathrm{f}^\mathrm{T}}\right)$ is the porosity-dependent heat conductivity (cf. *McKenzie*, 1984) with k_m^T, k_f^T the matrix and fluid heat conductivities, respectively, and the convective derivatives are defined as $\frac{\mathrm{D}_i\bullet}{\mathrm{D}t}{=}\frac{\partial\bullet}{\partial t}{+}\boldsymbol{v}_i\cdot\nabla\bullet$ with $i{=}\mathrm{f},\mathrm{m}$.

The first equation (1a) is the balance of mass of matrix (ice) while the second equation (1b) expresses the balance of mass of the mixture as a whole and indicates that even though the individual phases are considered incompressible (ρ_m=const., ρ_f=const.) the two-phase mixture behaves as a compressible material. The second two equations (1c, 1d) are the balances of linear momentum of fluid and matrix, respectively. The first two terms on the right-hand side of eq. (1d) are due to compositional (i.e. two-phase) and thermal buoyancy, respectively, while the third term originated from the gradient of dynamic pressure difference between the two phases ($\Delta P{=}P_\mathrm{m}{-}P_\mathrm{f}$) and can be interpreted as a viscous deformation with porosity-dependent bulk viscosity $\zeta{\sim}\frac{\mu_\mathrm{m}}{\phi}$ (cf. *Ricard et al.*, 2001). Finally, the last equation (1e) is the balance of energy of the mixture as a whole - we can consider only one energy balance due to the assumption of thermal equilibrium between the two phases. The appropriate values of material parameters are summarized in Table 1.

In certain applications, the presented physical model may be reduced by imposing the so-called 'zero compaction length approximation' (e.g. *Spiegelman*,

Symb.	Variable	Value	Unit
α_m	*ice thermal expansivity*	$1.6{\times}10^{-4}$	1/K
c_f	*heat capacity of water*	4180	J/kg/K
c_m	*heat capacity of ice*	2100	J/kg/K
$\lvert\mathbf{g}\rvert$	*surface gravity*	1.32	m/s^2
k_0	*permeability constant*	10^{-10}–10^{-8}	m^2
k_f^T	*water thermal conductivity*	0.56	W/m/K
k_m^T	*ice thermal conductivity*	2.3	W/m/K
L	*latent heat of melting of ice*	$333{\times}10^3$	J/kg
μ_f	*water shear viscosity*	$1.793{\times}10^{-3}$	Pa s
μ_m	*ice shear viscosity*	10^{13}–10^{15}	Pa s
D	*ice shell thickness*	30	km
ρ_f	*water density*	1000	kg/m^3
ρ_m	*ice density*	920	kg/m^3

Table 1: Model parameters. The magnitude of k_0 was estimated by comparing the theoretical model ($k(\phi){=}k_0\phi^2$) with the measured values, the chosen values of ice viscosity correspond to melting point viscosities (cf. *Tobie et al.*, 2003), and the ice shell thickness was picked out from the range of admissible thicknesses (cf. *Billings & Kattenhorn*, 2005).

1993) which can be obtained simply by neglecting the last two terms on the right-hand side of eq. (1d). The magnitude of these two terms determines the extent to which the deformation of the matrix affects the excess water pressure Π and via eq. (1c) also the fluid flow. Their neglection is possible in the physical setting in which the dynamic coupling between the fluid flow and matrix deformation is of small or no importance. In the zero compaction length approximation (and when neglecting the thermal buoyancy), the flow law for the fluid is rather simple and reads

$$c\boldsymbol{v}_{\mathrm{r}} = -(1-\phi)\phi\Delta\rho\mathbf{g} \ , \tag{2}$$

indicating that the fluid flow is driven solely by the (two-phase) buoyancy force. The neglection of the mechanical coupling between the two phases causes that the term of the highest differential order is omitted, and so the mathematical character of the problem changes - the solution can be expected to differ qualitatively from the fully mechanically coupled problem. Since in the dimensionless form of equations (1a)–(1e) a dimensionaless parameter $\mathscr{C}$ appears in front of the two coupling terms, we refer to this approximation as 'zero $\mathscr{C}$ approximation' in the following text.

The melting point of water ice is uniquely determined by pressure, temperature and composition. Since we consider the material to be pure water ice (containing no impurities), the state variables reduce to pressure and temperature. For given pressure-temperature conditions, ice can be present in two different states - **temperate ice** where temperature equals the (pressure) melting temperature (T=T_{M}) and some amount of interstitial liquid water is present (ϕ>0) and **cold ice** characterized by ice temperature below the melting point (T<T_{M}) and zero liquid water content (ϕ=0). In a **polythermal ice** layer that comprises regions of cold as well as temperate ice, the evolution of porosity ϕ and temperature T determines in which of the two states the ice is present.

In this thesis, we concentrated on two kinds of problems: (i) the gravity-driven extraction of a prescribed partially molten reservoir in a purely temperate ice layer and (ii) the formation and subsequent evolution of a partially molten reservoir in a polythermal ice layer. The numerical methods used to solve these problems are based on finite volume method (our own code written in FORTRAN90) and finite element method (code that uses a free FE software package FEniCS, http://fenicsproject.org). To verify the performance of developed codes several tests were performed.

3 Parametric studies in temperate ice shells

In order to assess the importance of physical parameters in the system of governing equations, we performed a series of numerical experiments in one and two dimensions. We focused on the effects of ice permeability, ice rheology, heating, surface tension and the compaction length. The main reason to investigate these effects is that some of the assumptions commonly used in the majority of multi-phase models, like the assumption of constant viscosity of the constituents, is probably invalid when dealing with complex materials such as ice. Expecting that the two-phase gravity driven transport exhibits formation of nonlinear wave trains (e.g. *Scott et al.*, 1986), large local space-temporal variations of porosity

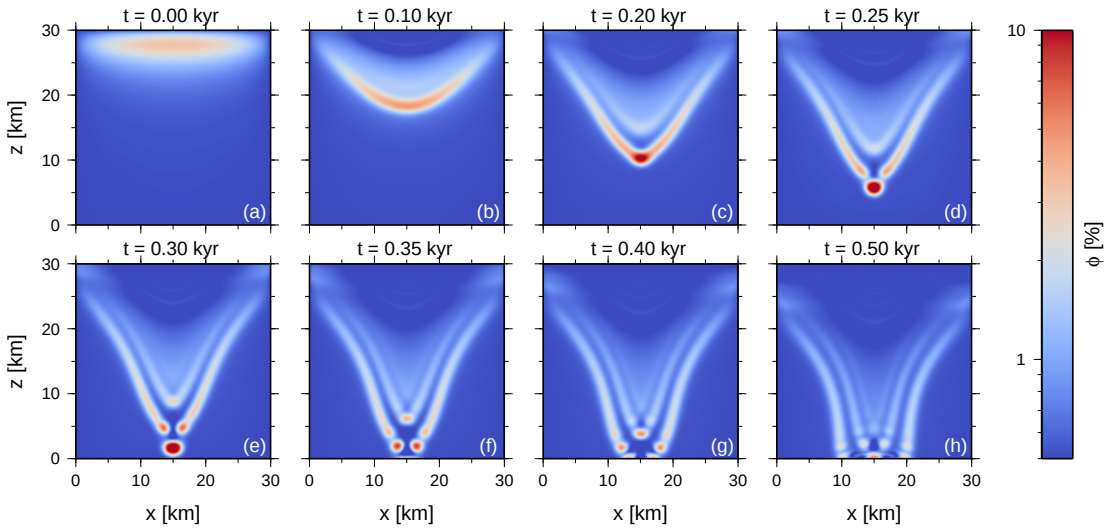

Figure 1: Snapshots of porosity evolution (with ϕ^{off}=0.5%) with the time increasing from left to right and from top to bottom. The initial condition (eq. 3) is depicted in panel a. The porosity scale is logarithmic. Computed with k_0=10^{-9} m^2 and μ_{m}=10^{13} Pa s, the other parameters are taken from Table 1.

would occur in the ice matrix. Since ice viscosity is highly sensitive to the amount of interstitial fluids present (*De La Chapelle et al.*, 1999), such porosity variations would inevitably induce significant viscosity variations.

In all experiments, we consider the following initial condition for porosity

$$\phi(x,z,0) = \frac{-10(z-1)}{1+(10(z-1))^4}\sin(\pi x) + \phi^{\text{off}} \ , \tag{3}$$

with ϕ^{off} a slight offset from zero (necessary for numerical reasons). This initial condition represents a subsurface partially molten reservoir. We also assumed constant (in space and time) melting temperature which led to zero thermal buoyancy in eq. 1d (since T_0=T_{M} and so ΔT=T_{M}−T_{M}=0) and eliminated the convective temperature derivatives in eq. (1e) - the energy balance then served solely to evaluate the melting rate r_{f}.

Figure 1 shows a few snapshots of the porosity evolution computed with ϕ^{off}=0.5% in two dimensions. We observe a rather efficient transport of meltwater by microscopic percolation through the temperate ice layer - apparently, porosity is transported downwards in the form of successive waves (wave train) formed due to the coupling between the fluid motion and the matrix deformation. Their wavelength is governed by the values of ice viscosity μ_{m} and permeability $k(\phi)$ - the higher the value of μ_{m} and/or $k(\phi)$, the larger the compaction length defined as

$$\delta = \sqrt{\frac{k(\phi)\left(\zeta+\frac{4}{3}\mu_{\text{m}}\right)}{\mu_{\text{f}}}} \ , \tag{4}$$

and thus the larger the wavelength (*Rabinowicz et al.*, 2002). While these characteristics of the flow are present also in the one-dimensional setting, certain new characteristics appear in two dimensions - contrary to one-dimensional simulations where only vertical motions were possible, in two dimensions water flows not only vertically but also in the inward direction leading to very strong melt

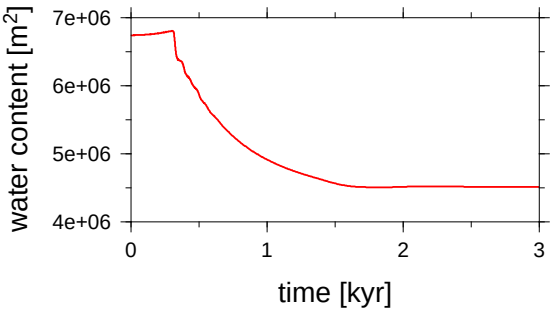

Figure 2: Time evolution of water content (porosity integrated throughout the domain). Computed for the same set of parameters as Figure 1.

localization (panel c) and even separation of a local porosity maxima (panels d and f). This melt localizing effect further enhances the melt flow velocity and so the porosity transport in two dimensions is slightly faster than in one dimension.

The majority of the initial water content (appart from the background value) is extracted from the layer within approximately 1 kyr (cf. Figure 2). The time needed to extract $1/e$ of the initial amount of water from the layer of thickness D can be estimated using the compaction time scale (*McKenzie*, 1989):

$$t_{\mathrm{D}} = \frac{D\mu_{\mathrm{f}}\phi}{k(\phi)\Delta\rho g} \ . \tag{5}$$

For ϕ∼3% (maximum amplitude at the beginning of the simulation) this formula yields the extraction time of approximately 0.5 kyr which (given the nonlinearity of the extraction process) agrees satisfactorily with the travel time of the first wave in our simulation (∼0.3 kyr).

The results of further numerical experiments (not depicted here) have shown that the ice permeability has the major impact on the time scale of water propagation (in agreement with eq. 5) and affects also the wavelength of porosity waves (cf. eq. 4). While the propagation velocity depends on permeability approximately linearly, with the extraction time scales ranging from less than one kiloyear for large permeabilities (k_0=10^{-8} m^2) to several kiloyears for small permeabilities (k_0=10^{-10} m^2), the wavelength scales with its square root. The value of permeability thus strongly influence the flow pattern on both local and global scale. Simulations with the 'percolation threshold' (that mimics the closure of the net of veins and microchannels in the matrix and subsequent drop in its connectivity observed in nature, cf. *Golden et al.*, 1998) revealed that even for very low permeability (caused by relatively large value of threshold ϕ_{c}=5%), water lens at the top of temperate ice layer is not stable and collapses down due to formation of gravitational (Rayleigh-Taylor-like) instability within approximately 10 kyr.

We also found that the ice rheology mainly influences the water flow on a local scale. The most important effect is the strong viscosity reduction due to porosity weakening, which enhances localization of waves and leads to a significant increase of peak porosity values. The inclusion of temperature and stress dependence has only moderate effect. Although the ice rheology affects the flow pattern on a local scale, the global scale transport properties, such as the characteristic time of propagation and the total meltwater volume, can be reasonably well reproduced by a constant viscosity model with values from the range of 10^{13}–5×10^{15} Pa s (that correspond to melting point viscosities).

The addition of volumetric heating as well as the increasing value of background porosity ϕ^{off} decrease the wave train propagation time while the heat source locallized above the initial porosity maximum increases the total amount

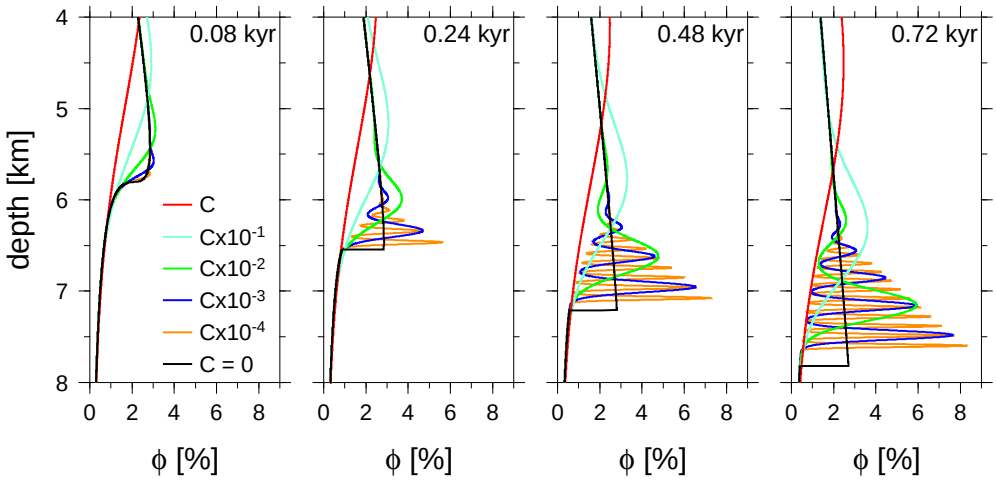

Figure 3: Snapshots of time evolution of porosity profiles for various values of $\mathscr{C}^i$ and zero $\mathscr{C}$ setting. Time increases from left to right and only vicinity of the shock is depicted. Computed for the same set of parameters as Figure 1.

of water in the ice shell but plays negligible role in the transport process. Concerning the effect of surface tension, we have numerically confirmed that it is negligible in the context of our physical setting.

We have also investigated the role of the dimensionless parameter $\mathscr{C}$ (in one dimension), which defines the strength of mechanical coupling between the phases and is related to the so-called compaction length. We numerically explored the relation between a zero compaction length model and the models where the coupling coefficient approaches zero. Figure 3 shows the evolution of the initial porosity profile (eq. 3 with x=1/2 and ϕ^{off}=0%) for five values of the parameter $\mathscr{C}^i=10^{-i}\mathscr{C}$, $i=0,1,2,3,4$, and for $\mathscr{C}$=0. In contrast to the non-zero $\mathscr{C}$ solution (all colors except for black) where a wave train evolves, for $\mathscr{C}$=0 (black color) a single porosity shock develops. Due to the reduction of the mechanical coupling between the phases, the propagation of the shock is faster than that of the wave train and also the peak porosities differ - while for $\mathscr{C}$=0 the porosity never exceeds the maximum initial value (∼3%), in the non-zero $\mathscr{C}$ case the amplitude of the wave train gradually grows to more than 8%. We also observe that with the gradually decreasing value of $\mathscr{C}^i$, the corresponding porosity profiles ϕ^i exhibit enhanced oscillations with shorter wavelength, while the time lag between the front wave and the position of the shock in the zero $\mathscr{C}$ solution decreases. This allows us to speculate that the zero $\mathscr{C}$ solution possibly corresponds to the weak limit (in the sense of distributions) of the non-zero $\mathscr{C}$ model, which seems to be supported by the numerical experiment (not shown here). The use of the zero compaction length model is thus misleading as far as the local character of the water flow is concerned while it may be appropriate for recovering the global (integral) transport properties.

In summary, we found that water transport through a 30 km thick temperate ice shell is very efficient with times necessary to deliver the majority of the initial water content to the bottom boundary ranging from less than one kiloyear to few tens of kiloyears. These results indicate that for the choice of material parameters used throughout this work, a large volume of water is not sustainable inside a fully temperate ice region.

4 Liquid water in Europa's ice shell: Results of numerical modeling

4.1 Transport of meltwater by two-phase flow in 1d

In the previous section we investigated the transport of a partially molten material through a temperate ice shell. However, in reality, when tidally-induced melting occurs at shallow depths, the underlying ice is not necessarily at the melting point. In such a case, the efficient melt extraction by two-phase flow might be delayed and occur only once the melting point is reached below. We now consider a polythermal ice shell and two different geophysical contexts which we implement by imposing specific initial temperature profiles and heating scenarios in one dimension. The first one corresponds to melting in the head of a hot plume (after *Sotin et al.*, 2002), while in the second one the melt is produced by shear motions on a strike-slip fault (after *Nimmo & Gaidos*, 2002).

As already discussed, viscosity of ice depends in general on numerous factors (such as temperature, stress, water content, etc.). Although strong viscosity variations can be expected in cold ice, their effect cannot be manifested in our 1d formalism. In temperate ice, the effect of temperature on viscosity is negligible (T=T_M), however, the influence of porosity (water content) can be significant. In the previous section we found that the global scale transport properties (e.g. water extraction time scale) can be reasonably well reproduced by a constant viscosity model and that the effect of ice viscosity on these properties is almost negligible. Since our main goal is the estimate of the extraction time scale, for the sake of simplicity, we consider a constant value of viscosity μ_m=10^{14} Pa s in our simulations. Besides viscosity, the other crucial parameter is the ice permeability, which has a major effect on the speed of porosity waves propagation (cf. compaction time scale, eq. 5). Since we are interested in the upper estimate for the water extraction time which determines the stability of the water reservoirs, we choose the minimum admissible value (k_0=10^{-10} m^2) of the ice permeability constant.

Melting in a hot plume

Since we cannot properly model thermal evolution of a hot plume in one-dimensional geometry, we approximate it by parametrizing the heat source as

$$Q_\mathrm{t} = H_\mathrm{t} - H_\mathrm{c} = xH_\mathrm{t} \ , \tag{6}$$

where H_t is the tidal heating and H_c stands for convective cooling. The scaling parameter x is typically equal to 10–20% of the tidal heating rate. Following *Tobie et al.* (2003), the viscosity-dependent tidal heating is expressed as:

$$H_\mathrm{t} = \frac{2H_\mathrm{t}^\mathrm{max}}{\mu_\mathrm{m}/\mu_\mathrm{m}^\mathrm{max} + \mu_\mathrm{m}^\mathrm{max}/\mu_\mathrm{m}} \ , \tag{7}$$

where $H_\mathrm{t}^\mathrm{max}$ is the maximum heating rate that occurs for viscosity $\mu_\mathrm{m}^\mathrm{max}$. We consider $H_\mathrm{t}^\mathrm{max}$=$5\times10^{-6}$ W m^{-3} that corresponds to the average estimate of the heating due to tides, and, only for the evaluation of tidal heating, temperature and porosity-dependent viscosity μ_m (cf. *Tobie et al.*, 2003).

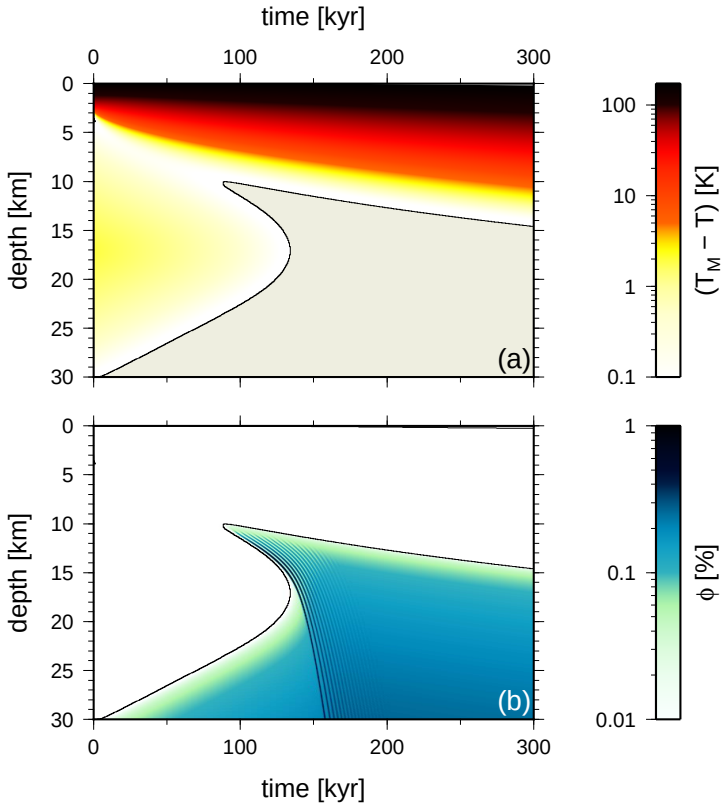

Figure 4: Hot plume set-up, x=15 %. (a) Space-time evolution of $T_{\mathrm{M}}-T$. The shaded region (corresponding to the colored region in panel b) marks the partially molten material at the melting temperature (temperate ice). (b) Space-time evolution of porosity. In both panels, the black contour represents the boundary between the temperate and cold ice.

The results for the hot plume simulation with x=15% and the model parameters given in Table 1 are depicted in Figure 4. Shortly after the beginning of the simulation, the melting temperature is reached only at the bottom boundary and melting just occurs at the base of the ice shell - the water produced there is immediately transported to the underlying ocean. The molten region where water can propagate spreads gradually from the bottom boundary to the head of the plume. At approximately 90 kyr, melting begins also at the depth of about 10 km and porosity waves start to develop. However, their migration is limited within the temperate ice region where temperature is at the melting point. Roughly 40 kyr later, both temperate regions connect, thus permitting an efficient transport of water all the way to the bottom boundary. Melting temperature is reached in approximately two thirds of the ice shell (Figure 4, panel a) but the value of porosity never exceeds 1% (Figure 4, panel b).

For higher values of x (20% and 30%), which correspond to less efficient convection and thus more efficient warming of the ice shell, the two distinct melting regions form again - since the tidal heating rate is higher, the melting starts earlier and more water is produced. However, both regions coalesce faster permitting earlier water outflow. When the value of x is decreased (to $\leq$10%), corresponding to enhanced convective cooling and slower warming of the ice shell, melting occurs only in the lower half of the ice shell and less water is produced. For all tested values of x (5–30%), the maximum porosity at shallow depth stays well below 1% and thus no water accumulates there.

Melting at the strike-slip fault

This set-up represents the process of melt production due to tidally-induced displacement along a strike-slip fault. In addition to the volumetric tidal heating

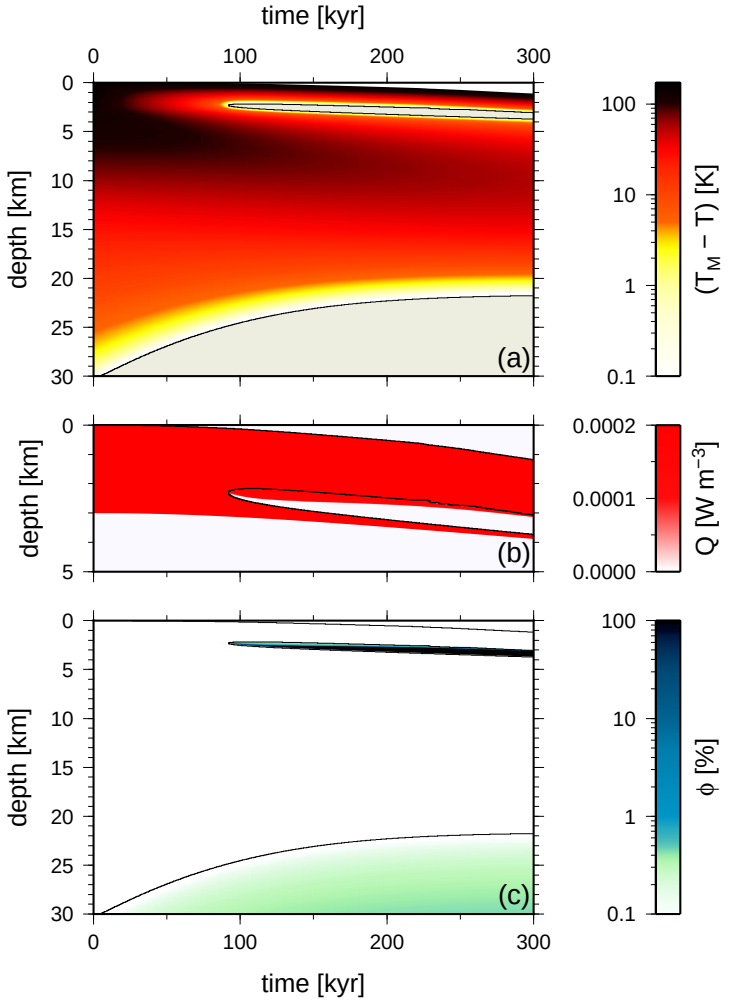

Figure 5: Strike-slip fault set-up, H_s=2×10^{-4} W m^{-3}, d_s=3 km and γ_s=45. (a) Space-time evolution of $T_M - T$. The shaded regions (corresponding to the colored regions in panel c) mark the partially molten material at the melting temperature. (b) Space-time evolution of the heating rate in the top 5 km. (c) Space-time evolution of porosity. As in Figure 4, the black contours represent the boundary between the temperate and cold ice.

H_t (eq. 7), we also include a localized heat source corresponding to shear heating along and just below a strike-slip fault (cf. *Nimmo & Gaidos*, 2002):

$$Q_s(d) = H_s \exp(-\gamma_s \phi) \qquad d \leq d_s \ . \tag{8}$$

Here H_s is the shear heating amplitude, d is the (variable) depth, d_s is the shear zone depth and γ_s is a weakening parameter (caused by the reduction of a friction coefficient due to melting, cf. *Oksanen & Keinonen*, 1982). The layer is assumed to be in a conductive state (no convective cooling, x=1).

The results for the strike-slip fault simulation with H_s=2×10^{-4} W m^{-3}, d_s=3 km and γ_s=45 are displayed in Figure 5 (with the values of other parameters taken from Table 1). As in the previous (hot plume) case, the first melt appears at the bottom boundary and the water flows freely from the domain to the underlying ocean without creating waves. After approximately 90 kyr, melting begins also at a depth of about 2 km where the melting temperature is reached due to the enhanced shear heating. Since the ice below is cold ($T \ll T_M$, Figure 5, panel a) and assumed free of fractures, no water propagates downward. Even though the heating in the subsurface temperate ice region decreases rapidly due to the increasing porosity (one order of magnitude reduction per 5% of porosity increase, Figure 5, panel b), the liquid water is trapped there and its amount gradually grows (Figure 5, panel c). As the initial temperature in the upper half of the ice shell is rather low and the volumetric heating (eq. 7) is not very efficient there,

the cold impermeable zone separating the subsurface water lens from the bottom temperate zone is preserved throughout the simulation (300 kyr).

Our numerical simulations also showed that for small shear-heating amplitude (H_s=5×10^{-5} W m^{-3}), no melt is produced at shallow depths (at least during 300 kyr) for 3 and 5 km thick shear zone. For moderate amplitude of heating (H_s=10^{-4} W m^{-3}) and deeper shear zone (d_s=5 km), a liquid water lens is created and remains stable for at least 100 kyr, but no water is produced for the same amplitude of heating and a more shallow shear zone (d_s=3 km). Increasing further the heating amplitude (H_s=2×10^{-4} W m^{-3}) enables melting also for a more realistic shear zone depth d_s=3 km (cf. *Nimmo & Gaidos*, 2002). These results are not affected by varying the value of the porosity weakening γ_s (eq. 8) - this parameter can slightly change the total amount of molten water but has a negligible effect on the maximum porosity in the shear zone and does not influence the time scale of liquid water extraction from shallow depths.

Discussion and summary

Our model is clearly limited by several assumptions. First of all, we assume a pure water system, while observations of colored hydrated materials within disrupted surface areas suggest that Europa's ice shell may contain a significant fraction of contaminants (e.g. *Zolotov & Kargel*, 2009) that could lower the melting point by several tens of Kelvins (*Pappalardo & Barr*, 2004). Their presence might have a large impact if they were located only in the upper part of the ice shell and promoted accumulation of concentrated brines at shallow depths as suggested by *Schmidt et al.* (2011). In this context, the volume of the accumulated salty water above a hot plume may be larger than in the case of a pure water system.

The assumed 1d geometry does not allow to solve for the lateral aspect of the problem and a 2d approach is necessary to describe the lateral flows, the development of convective instabilities and the potential effect of the upwelling ice velocity. Finally, our model neglects the effect of hydrofracturing. As discussed earlier, differences in physical settings make direct comparison between Earth's and Europa's hydrological system questionable. On Europa, the best candidate environment for nucleation and propagation of water-filled cracks would be in cold ice regions beneath a large volume of accumulated water (similar to what we obtain in the strike-slip fault set-up). A strong effect counterbalancing this mechanism would however be the fast freezing of water in such a cold environment. Both gravitational instabilities and hydrofracturing processes may become predominant only once a sufficient volume of water is accumulated. Further modeling is needed to evaluate the critical volume for which these processes dominate in Europa's ice shell conditions and to understand how they differ from those on the Earth. In any case, once activated, these processes would reduce the amount of accumulated water, and therefore the volumes reported here should be considered as upper limits.

Overall, our simulations showed that accumulation of a significant water volume above warm ice plumes is very unlikely, whereas it may be temporarily possible below recently active double ridges subjected to large strike-slip motions. Transient water accumulation ($\leq$100 kyr) and drainage may play a key role in the dynamics of Europa's ice shell and may be revealed by future exploration missions (*Grasset et al.*, 2013).

4.2 Gravitational stability of water lenses in 2d

In the previous part we have investigated the possibility of ice melting at shallow depths within Europa's shell for two geodynamic contexts and we have studied the stability of the newly-emerged meltwater lenses in one dimension, considering constant ice viscosity. This approach is limited by its one-dimensional character and can account neither for the lateral ice flows nor for the destabilization of larger water lenses due to formation of gravitational instability. Also the temperature evolution cannot be properly described in one dimension. Finally, ice viscosity is highly nonlinear and, for conditions within Europa's ice shell, probably far from constant. We now perform a similar study - while we considered only one-dimensional geometry and constant ice viscosity in the previous part, here we work in two dimensions and consider temperature-, porosity- and stress-dependent ice viscosity. On the other hand, a porous (two-phase) flow is now neglected (by setting the ice permeability to zero) - in this impermeable approximation, water is locked within the ice matrix and cannot percolate through microporous veins, but is rather advected with the ice. These two approaches thus complement each other - a more complex model that would fully couple the two-phase flow with the solid-state thermal convection will be considered in the future study. As before, we consider the two distinct melting scenarios.

Melting in a hot plume

In this part, volumetric tidal heating of the form given by eq. (7) is assumed while viscosity now depends on temperature, stress, porosity and grain size (which is kept constant throughout the simulations). We consider grain sizes from the range of 0.1–5.0 mm, that are plausible for Europa and allow convection to occur for Europa-like ice shell thicknesses (∼30 km) and realistic values of tidal heating rates (cf. *Han & Showman*, 2011). Following *Tobie et al.* (2003) we take $\mu_{\mathrm{m}}^{\mathrm{max}}$=1.5×10^{14} Pa s and vary H_{max} from 3 to 8×10^{-6} W m^{-3}. For all simulations in this section, domain of 60 km×30 km is considered and the viscosity contrast across the layer is approximately 10^{10} (no viscosity cut-off is applied) as a result of combined effect of strengthening towards the top boundary due to temperature decrease and weakening due to presence of melt within the partially molten areas. The implementation of viscosity cut-off could substantially modify our results and will be comprised in the future study.

Time evolution of porosity ϕ for d=0.7 mm and H_{max}=3×10^{-6} W m^{-3} is depicted in Figure 6. Melting starts within a central hot plume which is rather quickly (during ∼200 kyr) destabilized due to negative melt buoyancy (panels a–c). Melting then continues within two side plumes (panel d) and also within two central plumes that originated from the former central plume destabilized by melt (panel e). After approximately 1200 kyr from the onset of melting, a partially molten region covers the whole bottom boundary (panel f) with the surplus (w.r.t. the background value ϕ^{off}) maxima of about 6%. The maximum height occupied by some amount of partial material (ϕ>ϕ^{off}) is however <10 km.

To investigate the effect of grain size on the process of ice melting and subsequent water transport, we computed a couple of simulations with grain sizes ranging between 0.1 and 5 mm. At first, we considered d=1 mm - for this choice of grain size, the viscosity is rather high, the flow velocities are quite small and only relatively small hot plume develops. Melting temperature is reached within

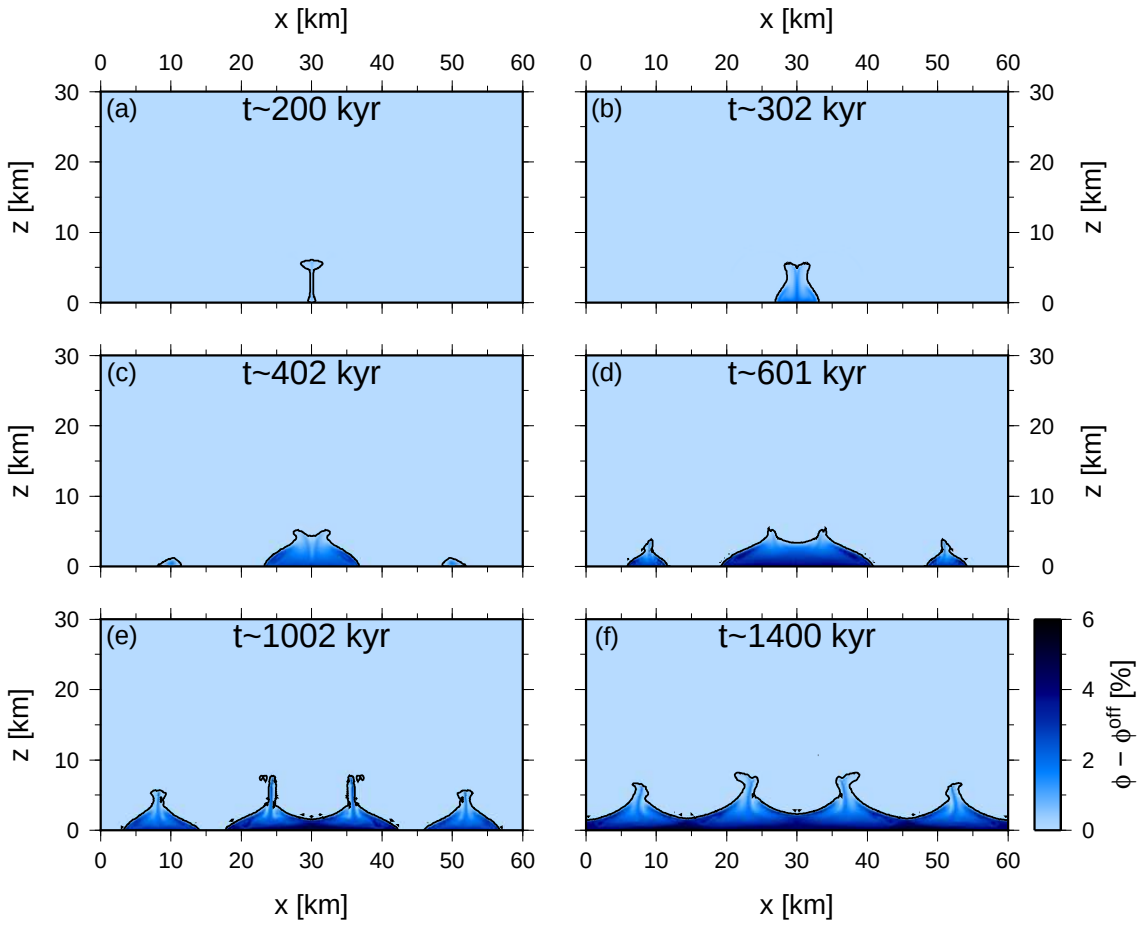

Figure 6: Snapshots of porosity for $H_{\max}$=3×10^{-6} W m^{-3} and d=0.7 mm. Time increases from left to right and from top to bottom. Black contours in porosity fields bound porosity larger than the background value (ϕ>$\phi^{\rm off}$).

∼200 kyr from the beginning of the simulation but melting occurs only within a few kilometers from the bottom boundary. For even larger grain size (d=5 mm), the Rayleigh number is too small to allow convection. Finally, for d=0.1 mm, which can be considered as a lower limit for Europan grain size, heating occurs outside the hot plumes and even for extremely large heating amplitudes of $H_{\max}$=8×10^{-6} W m^{-3} (that can be considered as an upper limit, cf. *Tobie et al.*, 2003), the melting temperature is not reached anywhere within the ice shell and thus no melt is produced.

Melting at the strike-slip fault

To describe heating produced by shear motions at the fault, we follow the approach of *Han & Showman* (2008) and assume a heat source of the form

$$Q_{\rm s} = H_{\rm s} \exp\left[-\left(\frac{x-x_0}{\sigma_{\rm x}}\right)^2 - \left(\frac{z-z_0}{\sigma_{\rm z}}\right)^2 \right] \Gamma_{\rm s}(\phi) \ , \qquad (9)$$

with $\Gamma_{\rm s}(\phi)$ the reduction of shear heating due to reduction of friction coefficient taken in a similar form as in eq. (8). Domain of 20 km×20 km is considered and the heat source (∼1 km wide and 2 km high) is placed near the top boundary in the middle (x_0=10 km) - this geometry is fixed in all simulations. Only temperature and porosity dependence of viscosity is assumed and the volumetric heating of the form given by eq. (7) is included in some simulations.

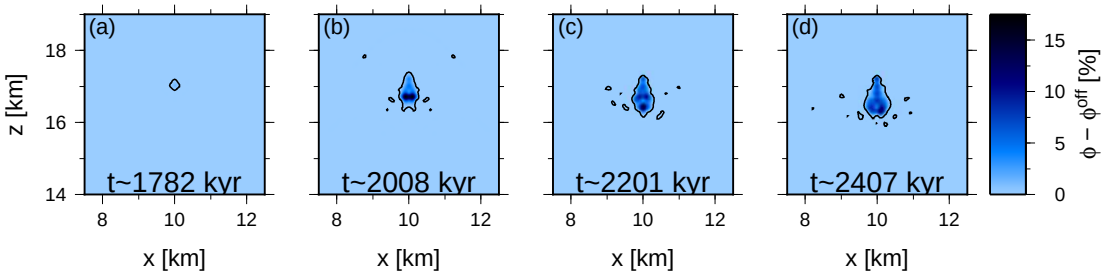

Figure 7: Time evolution of porosity for simulation with H_s=2×10^{-4} W m^{-3} and no volumetric heating. Only cut-out detail ($x \in \langle 7.5, 12.5 \rangle$ km and $z \in \langle 14, 19 \rangle$ km) is shown for better clarity. Time increases from left to right. Black contours in porosity fields bound porosity larger than the background value ($\phi > \phi^{off}$).

Figure 8: Viscosity at the end of simulations computed with H_s=2×10^{-4} W m^{-3} and H_{max}=0 (panel a) or H_{max}=2×10^{-6} W m^{-3} (panel b). The black contour marks the viscosity at the melting point.

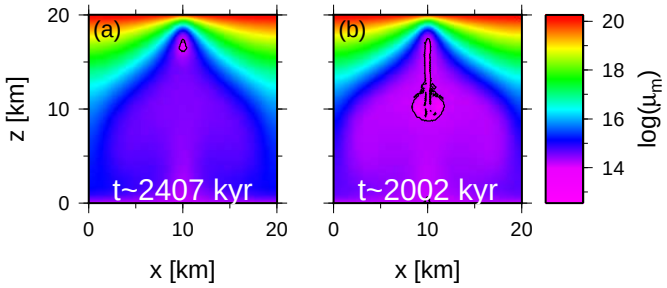

At first, we investigate the effect of shear heating amplitude H_s. Based on results of *Nimmo & Gaidos* (2002), we choose two values, H_s=10^{-4} and H_s=2×10^{-4} W m^{-3}. Initially, we do not consider any volumetric tidal heating, i.e. Q=Q_s. In the case with weaker shear heating amplitude, H_s=10^{-4} W m^{-3}, the melting temperature is not reached even after ∼6700 kyr from the start of the simulation, while in simulation with larger shear heating, H_s=2×10^{-4} W m^{-3}, the melting temperature is reached after ∼1800 kyr at just ∼3 km below the surface. The subsequent evolution of porosity is depicted in Figure 7 and suggests that (for this model setting) a partially molten lens with surplus porosity (w.r.t. ϕ^{off}) of about 10–15% can form approximately 3 km below the surface and remain stable for at least 600 kyr. The stability of this partially molten region is due to viscosity increase of approximately one order (from ∼10^{14} to ∼10^{15} Pa s) just below the molten lens (cf. Figure 8, panel a).

We now study the effect of the addition of volumetric heating to shear heating, i.e. we consider Q=Q_s+Q_t in the energy balance. The shear heating amplitude is kept at H_s=2×10^{-4} W m^{-3} and the volumetric heating of amplitude H_{max}=2×10^{-6} W m^{-3} is considered. For these values, melting temperature is reached after approximately 1440 kyr at depth of about 3 km from the surface, as in the previous case. Contrary to the previous case, the internal temperature increases due to the run-away effect of volumetric heating - once the temperature increases, the corresponding viscosity decreases leading to stronger heating and so on. Therefore, at the end of simulation (at t∼2002 kyr), the temperature of the large part of the computational domain is well above 250 K with corresponding viscosities of the order of 10^{14} Pa s or less (cf. Figure 8, panel b). The corresponding porosity evolution is shown in Figure 9 - we observe the creation of a partially molten lens of a few percents during approximately 160 kyr (panels a,

b) and its relatively rapid destabilization due to its negative buoyancy within less than 200 kyr (panel c) with the subsequent water transport towards the bottom boundary (panel d).

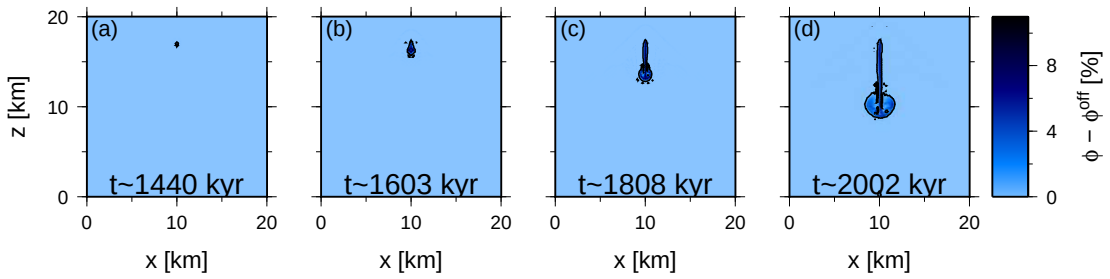

Figure 9: The same as in Figure 7 but with volumetric heating of amplitude $H_{\max}=2\times10^{-6}$ W m^{-3}.

Summary and discussion

We have investigated the possibility of the onset of melting within the ice shell of Europa in two geodynamical contexts and two-dimensional geometry. In the case of tidally-heated hot plumes, melting temperature is easily reached for the majority of appropriate physical parameters, but melting mostly occurs within the lower half of the ice shell. Even if some melt is produced at the top of hot plume, it is still located at least 10 km below the surface due to the presence of a thick conductive lid at the top of computational domain. Moreover, even small amounts of melt ($\sim$ few percents above the background value ϕ^{off}) cause relatively quick destabilization of the ascending hot plumes and their collapse towards the bottom boundary within approximately 100–200 kyr. Our results thus agree with the results of *Tobie et al.* (2003) and indicate that accumulation of partial melt close to the surface is not likely in this context.

In the case of tidally-activated strike-slip fault, melting temperature might be reached very close to the surface ($\sim$3 km) for large amplitudes of shear heating of at least $H_{\text{s}}=2\times10^{-4}$ W m^{-3}. Our results indicate that if the layer below the fault is not internally heated, a small lens of partially molten material can be stable for at least 600 kyr. On the other hand, if the underlying layer is tidally heated, this lens is quickly destabilized (with the destabilization rates depending on the heating amplitude).

All our simulations neglect the possible drainage of water through the process of hydrofracturing. As already mentioned, we do not consider this transport mechanism to be responsible for water drainage within Europa's ice shell. If the fractures developed after all, they might drain the accumulated water rather quickly through the formation of a macroscopic system of crevasses - in this sense, the lifetimes of partially molten lenses provided in this chapter might be considered as upper estimates. Similarly, the presence of a possibly significant fraction of melting-temperature lowering salts is neglected in the current work. Apart from the effects on the melting temperature of ice, the presence of salts would also influence its buoyancy, leading to a coupled thermo-compositional (two-phase) convection problem.

Conclusions and perspectives

In this work, we have investigated the conditions under which water can be generated and transported within the ice shell of Europa. For this purpose, we have adapted the theory of two-phase flow to the conditions of Europa's ice shell and we have developped numerical tools in 1d and 2d geometry to quantify the water accumulation and transport for different melting scenarios.

Using the current knowledge about Europa and the analogy with water transport in terrestrial glaciers, we identified the main geodynamical contexts under which water may be generated on Europa and we related them with the expected transport mechanisms. Due to its eccentric orbit around Jupiter, the tidal dissipation has a strong impact on the thermal structure of Europa's ice shell. Assuming that the ice shell is in the convective regime, the thermally-reduced viscosity in the ascending hot plumes may significantly increase the heating rates and lead to runaway melting as suggested by *Sotin et al.* (2002). In this case, melting would occur within the convective portion of the ice shell. According to the findings of *Nimmo & Gaidos* (2002), shear motions along tidally-activated strike-slip faults result in a very localized and strong heat source located only a few kilometers below Europa's cold surface, which might eventually lead to shallow melting within the topmost, brittle part of the shell. Given the anticipated conditions in these two geodynamical contexts, we do not expect crevasse hydrofracturing, a dominant mechanism within the Earth's glaciers responsible for annual water drainage, to be widely present within Europa's ice shell. Instead, we argue that microporous flow of liquid water, similar to magma percolation within the Earth's mantle and mathematically described by two-phase mixture equations, could be responsible for draining the potential water reservoirs together with a possible formation of gravitational (Rayleigh-Taylor-like) instabilities.

Following the approach of *Drew* (1983), *Drew & Passman* (1999), *Bercovici et al.* (2001) and *Šrámek et al.* (2007), we proposed a detailed derivation of two-phase equations for the particular case of mixture of water ice and liquid water. The numerical tools developed and used throughout this thesis are based on finite volume and finite element methods and were carefully tested.

We performed parametric studies of water transport through the temperate ice shell in one and two dimensions. In this setting, the temperature of the shell is constant in time and equal to the (pressure) melting temperature. We investigated the role of several material parameters on the liquid water transport and found that the key role in this process is played by the ice permeability which affects both, the local and global characteristics of water transport by controlling the time scale of the process as well as strongly influencing the wavelength. A similar effect on the local scale (in terms of wavelength) was also found for the ice viscosity. Yet, viscosity has almost negligible effect on the time scale of the process. Moreover, we have found that the very complex ice rheology can be in numerical simulations of two-phase flow in our planetary setting approximated by a constant viscosity from the range of 10^{13} to 5×10^{15} Pa s. Finally, the mechanical coupling between the two phases was found to be important, especially when the local character of flow is of interest. Overall, the results of this parametric study indicate that partially molten reservoirs are not gravitationally stable in the temperate ice shells and that the liquid water is rather quickly (within less

than a few tens of kiloyears) delivered to the underlying water ocean.

Finally, we investigated the onset of melting and the subsequent water evolution within the ice shell of Europa in the two melting scenarios. We performed a one-dimensional study where the transport of meltwater was enabled in the temperate parts of the ice shell by porous (two-phase) flow and a two-dimensional study where we only considered the impermeable limit of two-phase equations. In the latter case, all the liquid water was locked within the ice and advected with it. These studies are complementary in the assumed transport mechanism (porous flow vs. gravitational instability) and can be both considered as the first steps towards a more complicated model that would couple these two approaches.

In the case of tidally-heated hot plumes, we found that melting could initiate within an ascending hot plume even for relatively small amplitude of tidal heating of 3×10^{-6} W m^{-3} for moderate values of grain size (d=0.5–1 mm). For larger value of grain size, d=5 mm, convection does not initiate (shell thickness of 30 km is considered) and for the smallest grain size used (d=0.1 mm) convection develops but melting temperature is not reached. If initiated, melting occurs at the bottom boundary as well as at the top of hot plumes several kilometers below the surface. In the one-dimensional simulations with porous flow, the ice below the partially molten area soon reaches the melting temperature and thus enables very efficient microporous transport of water towards the underlying ocean. In the two-dimensional simulations without porous flow, the partially molten material from the plumes is not gravitationally stable and even small melt fractions of a few percents are very quickly destabilized and within less than a few hundreds of kiloyears collapse down towards the bottom boundary. Our two-dimensional results thus qualitatively agree with those computed in one dimension even though different transport mechanisms (gravitational instability and porous flow, respectively) were considered. These results indicate that the accumulation of partial melt or even liquid water within few kilometers of Europa's surface is very unlikely in this context, at least if the ice shell is free of melting-temperature-lowering contaminants. The efficient water drainage suggested by our results might play an important role in the dynamics of Europa's ice shell and even assure the connection between Europa's shallow subsurface and the deep ocean.

In the case of tidally-activated strike-slip fault, we found that melting could initiate approximately 3 km below the surface for a local heat source of at least 2×10^{-4} W m^{-3}, leading to accumulation of a substantial amount of water. The newly created partially molten domain with maxima of $\sim$10–20% can remain stable this close to the surface for at least 600 kyr if the underlying ice shell is not tidally heated from within. For volumetric tidal heating with amplitudes from the range of 2–5×10^{-6} W m^{-3}, the results of our studies differ. While in one dimension we found that a large amount of water might accumulate and remain stable only a few kilometers below the surface for several hundreds of kiloyears even for the interior heating as high as 5×10^{-6} W m^{-3}, the results of two-dimensional simulations showed that the partially molten reservoir is not gravitationally stable and collapses down within $\lesssim$200 kyr even for smaller amplitude of volumetric heating (2×10^{-6} W m^{-3}). Overall, our simulations suggest that a partially molten lens or even a liquid water reservoir might form below recently active strike-slip faults and remain (gravitationally) stable for at least several hundreds of kiloyears if the underlying ice is free of fractures and not

tidally heated from within (and thus sufficiently cold and viscous). These lenses might coincide with the sills advocated by *Dombard et al.* (2013) as a necessary ingredient to produce the morphology of Europa's ubiquitous double ridges.

Several improvements of the developed numerical tool are already intended. First of all, the relaxation of the zero permeability assumption will enable the microporous transport of liquid water through the temperate parts of the shell, leading to a fully coupled model of the two-phase flow with the classic solid-state thermal convection. Europa's scarred surface represents an evidence of the brittle behavior - the implementation of viscosity cut-off as a rough approximation of the brittle rheology might substantially modify our current results and will be considered in the next step. Similarly, the presence of salty contaminants might have effect on the melt generation and potential water accumulation. The extension of the current model to two-phase thermo-chemical convection by adding the salinity evolution and implementing the effect of salt on the melting temperature and buoyancy will be considered. Finally, minor adjustments will allow to use the developed numerical tool to investigate meltwater generation and its following evolution also within the ice shells of other satellites.

Acknowledgements

This research received funding from the European Research Council under the European Community's Seventh Framework Programme FP7/2007-2013 grant agreement 259285. Support from Charles University through projects SVV-2012-265308, SVV-2013-267308, and SVV-2014-260096 is thankfully acknowledged. This work was also supported by the IT4Innovations Centre of Excellence project (CZ.1.05/1.1.00/02.0070), funded by the European Regional Development Fund and the national budget of the Czech Republic via the Research and Development for Innovations Operational Programme, as well as Czech Ministry of Education, Youth and Sports via the project Large Research, Development and Innovations Infrastructures (LM2011033).

References

Anderson, J. D., G. Schubert, R. A. Jacobson, E. L. Lau, W. B. Moore, and W. L. Sjogren (1998), Europa's Differentiated Internal Structure: Inferences from Four Galileo Encounters, *Science*, **281**(5385), 2019–2022, doi:10.1126/science.281.5385.2019.

Barr, A. C., and R. T. Pappalardo (2005), Onset of convection in the icy Galilean satellites: Influence of rheology, *J. Geophys. Res.*, **110**(E12), doi:10.1029/2004JE002371.

Bercovici, D., Y. Ricard, and G. Schubert (2001), A two-phase model for compaction and damage: 1. General Theory, *J. Geophys. Res.*, **106**(B5), 8887–8906, doi:10.1029/2000JB900430.

Bierhaus, E. B., K. Zahnle, and C. R. Chapman (2009), Europa's crater distributions and surface ages, in *Europa* (eds. R. T. Pappalardo, W. B. McKinnon, and K. Khurana), The University of Arizona Press, Tucson, 161–180.

Billings, S. E., and S. A. Kattenhorn (2005), The great thickness debate: Ice shell thickness models for Europa and comparisons with estimates based on flexure at ridges, *Icarus*, **177**(2), 397–412, doi:10.1016/j.icarus.2005.03.013.

Birchwood, R. A., and D. L. Turcotte (1994), A unified approach to geopressuring, low-permeability zone formation, and secondary porosity generation in sedimentary basins, *J. Geophys. Res.*, **99**(B10), 20051–20058, doi:10.1029/93JB02388.

Blatter, H., and K. Hutter (1991), Polythermal conditions in Arctic glaciers, *J. Glaciol.*, **37**(126).

Carr, M. H., M. J. S. Belton, C. R. Chapman, M. E. Davies, P. Geissler, R. Greenberg, A. S. McEwen, B. R. Tufts, R. Greeley, R. Sullivan, J. W. Head, R. T. Pappalardo, K. P. Klaasen, T. V. Johnson, J. Kaufman, D. Senske, J. Moore, G. Neukum, G. Schubert, J. A. Burns, P. Thomas, and J. Veverka (1998), Evidence for a subsurface ocean on Europa, *Nature*, **391**(6665), 363–365, doi:10.1038/34857.

Collins, G., and F. Nimmo (2009), Chaotic terrain on Europa, in *Europa* (eds. R. T. Pappalardo, W. B. McKinnon, and K. Khurana), The University of Arizona Press, Tucson, 259–281.

De La Chapelle, S., H. Milsch, O. Castelnau, and P. Duval (1999), Compressive creep of ice containing a liquid intergranular phase: rate-controlling processes in the dislocation creep regime, *Geophys. Res. Lett.*, **26**(2), 251–254, doi:10.1029/1998GL900289.

Dombard, A. J., G. W. Patterson, A. P. Lederer, and L. M. Prockter (2013), Flanking fractures and the formation of double ridges on Europa, *Icarus*, **223**(1), 74–81, doi:10.1016/j.icarus.2012.11.021.

Drew, D. A. (1983), Mathematical modeling of two-phase flow, *Ann. Rev. Fluid Mech.*, **15**, 261–291, doi:10.1146/annurev.fl.15.010183.001401.

Drew, D. A., and S. L. Passman, *Theory of Multicomponent Fluids*, Appl. Math. Sci., **135**, Springer-Verlag, New York, 1999.

Durham, W. B., L. A. Stern, and S. H. Kirby (2001), Rheology of ice I at low stress and elevated confining pressure, *J. Geophys. Res.*, **106**(6), 11031–11042, doi:10.1029/2000JB900446.

Golden, K. M., S. F. Ackley, and V. I. Lytle (1998), The Percolation Phase Transition in Sea Ice, *Science*, **282**(5397), 2238–2241, doi: 10.1126/science.282.5397.2238.

Goldsby, D. L., and D. L. Kohlstedt (2001), Superplastic deformation of ice: Experimental observations, *J. Geophys. Res.*, **106**(B6), 11017–11030, doi:10.1029/2000JB900336.

Grasset, O., M. K. Dougherty, A. Coustenis, E. J. Bunce, C. Erd, D. Titov, M. Blanc, A. Coates, P. Drossart, L. N. Fletcher, H. Hussmann, R. Jaumann, N. Krupp, J.-P. Lebreton, O. Prieto-Ballesteros, P. Tortora, F. Tosi, and T. Van Hoolst (2013), JUpiter ICy moons Explorer (JUICE): An ESA mission to orbit Ganymede and to characterise the Jupiter system, *Planet. Space Sci.*, **78**, 1–21, doi:10.1016/j.pss.2012.12.002.

Han, L., and A. P. Showman (2008), Implications of shear heating and fracture zones for ridge formation on Europa, *Geophys. Res. Lett.*, **35**(3), L03202, doi: 10.1029/2007GL031957.

Han, L., and A. P. Showman (2011), Coupled convection and tidal dissipation in Europa's ice shell using non-Newtonian grain-size-sensitive (GSS) creep rheology, *Icarus*, **212**(1), 262–267, doi:10.1016/j.icarus.2010.11.034.

Hand, K. P., C. F. Chyba, J. C. Priscu, R. W. Carlson, and K. H. Nealson (2009), Astrobiology and the potential for life on Europa, in *Europa* (eds. R. T. Pappalardo, W. B. McKinnon, and K. Khurana), The University of Arizona Press, Tucson, 589–629.

Hansen, C. J., L. Esposito, A. I. F. Stewart, J. Colwell, A. Hendrix, W. Pryor, D. Shemansky, and R. West (2006), Enceladus' water vapor plume, *Science*, **311**(5766), 1422–1425, doi:10.1126/science.1121254.

Hutter, K. (1993), Thermo-mechanically coupled ice-sheet response - cold, polythermal, temperate, *J. Glaciol.*, **39**(131), 65–86.

Kattenhorn, S. A., and T. Hurford (2009), Tectonics of Europa, in *Europa* (eds. R. T. Pappalardo, W. B. McKinnon, and K. Khurana), The University of Arizona Press, Tucson, 199–236.

Khurana, K. K., M. G. Kivelson, D. J. Stevenson, G. Schubert, C. T. Russell, R. J. Walker, and C. Polanskey (1998), Induced magnetic fields as evidence for subsurface oceans in Europa and Callisto, *Nature*, **395**(6704), 777–780, doi:10.1038/27394.

Krawczynski, M. J., M. D. Behn, S. B. Das, and I. Joughin (2009), Constraints on the lake volume required for hydro-fracture through ice sheets, *Geophys. Res. Lett.*, **36**(L10501), doi:10.1029/2008GL036765.

McCord, T.B., G. B. Hansen, F. P. Fanale, R. W. Carlson, D. L. Matson, T. V. Johnson, W. D. Smythe, J. K. Crowley, P. D. Martin, A. Ocampo, C. A. Hibbitts, J. C. Granahan, and the NIMS Team (1998), Salts on Europa's surface detected by Galileo's Near Infrared Mapping Spectrometer, *Science*, **280**(5367), 1242–1245,

doi:10.1126/science.280.5367.1242.

McKenzie, D. (1984), The generation and compaction of partially molten rock, *J. Petrol.*, **25**(3), 713–765.

McKenzie, D. (1989), Some remarks on the movement of small melt fractions in the mantle, *Earth Planet. Sci. Lett.*, **95**(1-2), 53–72, doi:10.1016/0012-821X(89)90167-2.

Nimmo, F., and E. Gaidos (2002), Strike-slip motion and double ridge formation on Europa, *J. Geophys. Res.*, **107**(E4), 5021, doi:10.1029/2000JE001476.

Nimmo, F., and M. Manga (2009), Geodynamics of Europa's icy shell, in *Europa* (eds. R. T. Pappalardo, W. B. McKinnon, and K. Khurana), The University of Arizona Press, Tucson, 381–404.

Ojakangas, G. W., and D. J. Stevenson (1989), Thermal State of an Ice Shell on Europa, *Icarus*, **81**(2), 220–241, doi:10.1016/0019-1035(89)90052-3.

Oksanen, P., and J. Keinonen (1982), The mechanism of friction of ice, *Wear*, **78**(3), 315–324, doi:10.1016/0043-1648(82)90242-3.

Pappalardo, R. T., and A. C. Barr (2004), The origin of domes on Europa: The role of thermally induced compositional diapirism, *Geophys. Res. Lett.*, **31**(L01701), doi:10.1029/2003GL019202.

Rabinowicz, M., Y. Ricard, and M. Grégoire (2002), Compaction in a mantle with a very small melt concentration: Implications for the generation of carbonatitic and carbonate-bearing high alkaline mafic melt impregnations, *Earth Planet. Sci. Lett.*, **203**(1), 1205–1220, doi:10.1016/S0012-821X(02)00836-1.

Ricard, Y., D. Bercovici, and G. Schubert (2001), A two-phase model for compaction and damage: 2. Applications to compaction, deformation, and the role of interfacial surface tension, *J. Geophys. Res.*, **106**(B5), 8907–8924, doi:10.1029/2000JB900431.

Ricard, Y., O. Šrámek, and F. Dubuffet (2009), A multi-phase model of runaway core-mantle segregation in planetary embryos, *Earth Planet. Sci. Lett.*, **284**(1–2), 144–150, doi:10.1016/j.epsl.2009.04.021.

Roth, L., J. Saur, K. D. Retherford, D. F. Strobel, P. D. Feldman, M. A. McGrath, and F. Nimmo (2014), Transient water vapor at Europa's south pole, *Science*, **343**(171), doi:10.1126/science.1247051.

Schmidt, B. E., D. D. Blankenship, G. W. Patterson, and P. M. Schenk (2011), Active formation of chaos terrain over shallow subsurface water on Europa, *Nature*, **479**(7374), 502–505, doi:10.1038/nature10608.

Scott, D. R., and D. J. Stevenson (1986), Magma ascent by porous flow, *J. Geophys. Res.*, **91**, 9283–9296.

Scott, D. R., D. J. Stevenson, and J. A. Whitehead (1986), Observations of solitary waves in a viscously deformable pipe, *Nature*, **319**, 759–761.

Sotin, C., J. W. Head, and G. Tobie (2002), Europa: Tidal heating of upwelling thermal plumes and the origin of lenticulae and chaos melting, *Gephys. Res. Lett.*, **29**(8), 1233, doi:10.1029/2001GL013844.

Sotin, C., G. Tobie, J. Wahr, and W. B. McKinnon (2009), Tides and tidal heating on Europa, in *Europa* (eds. R. T. Pappalardo, W. B. McKinnon, and K. Khurana), The University of Arizona Press, Tucson, 85–117.

Spiegelman, M. (1993), Flow in deformable porous media I: Simple analysis, *J. Fluid. Mech.*, **247**, 17–38, doi:10.1017/S0022112093000369.

Šrámek, O., Y. Ricard, and D. Bercovici (2007), Simultaneous melting and compaction in deformable two-phase media, *Geophys. J. Int.*, **168**(3), 964–982, doi:10.1111/j.1365-246X.2006.03269.x.

Šrámek, O., Y. Ricard, and F. Dubuffet (2010), A multiphase model of core formation, *Geophys. J. Int.*, **181**(1), 198–220, doi:10.1111/j.1365-246X.2010.04528.x.

Tobie, G., G. Choblet, and C. Sotin (2003), Tidally heated convection: Constraints on Europa's ice shell thickness, *J. Geophys. Res.*, **108**(E11), 5124, doi:10.1029/2003JE002099.

Zolotov, M. Y., and J. S. Kargel (2009), On the Composition of Europa's Icy Shell, Ocean and Underlying Rocks, in *Europa* (eds. R. T. Pappalardo, W. B. McKinnon, and K. Khurana), The University of Arizona Press, Tucson, 431–457.

Author's publications and citation report

Related with the thesis topic

1. Souček, O., **K. Kalousová**, and O. Čadek (2014), Water transport in planetary ice layers - a parametric study, *Geophys. Astro. Fluid*, **108**(6), 639–666, doi:10.1080/03091929.2014.969251.
2. **Kalousová, K.**, O. Souček, G. Tobie, G. Choblet, and O. Čadek (2014), Ice melting and downward transport of meltwater by two-phase flow in Europa's ice shell, *J. Geophys. Res. Planets*, **119**(3), 532–549, doi:10.1002/2013JE004563.
    - Romero-Wolf, A., S. Vance, F. Maiwald, E. Heggy, P. Ries, and K. Liewer (2014), A Passive Probe for Subsurface Oceans and Liquid Water in Jupiter's Icy Moons, arXiv:1404.1876.
3. **Kalousová K.**, O. Souček, and O. Čadek (2012), Two-phase Convection in Icy Satellites, *Acta Universitatis Carolinae*, **53**(1), 61-71.

Not-related with the thesis topic

4. **Kalousová, K.**, O. Souček, and O. Čadek (2012), Deformation of an elastic shell with variable thickness: a comparison of different methods, *Geophys. J. Int.*, **190**(2), 726–744, doi:10.1111/j.1365-246X.2012.05539.x.
    - Dumoulin, C., O. Čadek, and G. Choblet (2013), Predicting surface dynamic topographies of stagnant lid planetary bodies, *Geophys. J. Int.*, **195**(3), 1494–1508, doi:10.1093/gji/ggt363.